

EXPERIMENTAL DERIVATION OF NEPHELINE SYENITE AND PHONOLITE
LIQUIDS BY PARTIAL MELTING OF UPPER MANTLE PERIDOTITES

Didier LAPORTE, Sarah LAMBART, Pierre SCHIANO, and Luisa OTTOLINI

SUPPLEMENTARY MATERIAL

1. Experimental and analytical techniques

1.1 Starting materials. The starting material used to prepare our two fertile mantle compositions was a fresh spinel lherzolite xenolith (Bri3) from Mont Briançon volcano, French Massif Central. Because a fine grain size is critical to attain chemical equilibrium, lherzolite Bri3 was first pulverized in a micronizing mill for 30 min to reduce its grain size to 2-4 μm . The powder was then fired 5 hours at 900°C in a CO_2/H_2 atmosphere with gas flow rates adjusted to yield an oxygen fugacity between the magnetite-wüstite and the iron-wüstite buffers ($f_{\text{O}_2} = 10^{-15.91}$ bar). As Bri3 contains only 100 ppm K_2O , small amounts of synthetic basalt B2 were added to Bri3 to prepare the fertile mantle compositions MBK (410 ppm K_2O) and MBK+ (930 ppm K_2O ; compositions Bri3, B2, MBK and MBK+ are given in Table 1). Mixtures of Bri3 and B2 were homogenized by grinding in an agate mortar for one hour.

The starting material for reversal experiments MBK+13 and MBK+14 was a mixture of 80.16 % MBK+ and 19.84 % phonolite gel +6 (Table 1). Phonolite gel +6 was prepared using the gel method (Luth and Ingamells, 1965), and then fired at the same T and f_{O_2} as lherzolite Bri3. Gel +6 matches well the target composition (that is, the glass in partial melting experiment MBK+6), except that it is ≈ 10 % richer in Na_2O .

1.2 Experimental techniques. The experiments were made in a non end-loaded, 3/4-inch piston-cylinder apparatus. We used double containers made of a graphite crucible fitted into a platinum capsule. The graphite container was loaded with 20-25 mg of starting powder, and then put into the platinum capsule and covered with a graphite lid. After loading, the capsule was dried in an oven at 300°C for 24 hours and then rapidly welded shut while still hot. For the series with composition MBK at 1.3 GPa, we used exactly the same technique as Laporte et al. (2004). For the series with MBK at 1 GPa and MBK+ at 1.3 GPa, an extra effort was made to minimize the amount of adsorbed water (Lambart et al., 2009): all the pieces of the piston-cylinder assemblies were fired at high temperature (from 400°C for graphite and pyrex, to 1000°C for crushable MgO), and then stored at 150°C. Just before an experiment, the full assemblage was fired a last time 24h at 300 °C. Ion probe measurements of water in experimental glasses (see below) show that the water content is strongly sensitive to melt fraction, and that our extra effort to minimize water contamination had only a marginal effect on the final water content. As a result, the relationship between water content of experimental glasses and melt fraction F (both in wt. %) for our whole data set (9 partial melting experiments, including three from Laporte et al., 2004) can be described by a single law:

$$\text{H}_2\text{O} = 1.350e^{-0.176 F}$$

with a coefficient of determination equal to 0,983.

1.3 Analytical techniques. The textures and parageneses of the run products were characterized using a JEOL JSM-5910 LV scanning electron microscope (Fig. 1; Supplementary Figs. S1, S3). Phase compositions were analysed with a Cameca SX-100 electron microprobe. For crystalline phases, a 15-kV accelerating voltage, a 15 nA beam current, counting times of 10 s, and a focussed beam were used. For glass analyses, the beam

current was lowered to 8 nA and a beam size of 5 μm was used whenever possible. When the glass-filled microdikes in the graphite container were only a few micrometers thick, a beam diameter of 2 μm was used. A comparison of the average Na_2O concentrations obtained with a 2 μm versus a 5 μm beam size in samples with large microdikes or large melt pools (such as reversal experiments) shows that a correction for sodium loss is required when a 2 μm beam size is used, and that this correction increases with increasing Na_2O concentration : the correction is + 2% for Na_2O concentrations of $\approx 5\%$ and + 4% for concentrations of 7-8 % (that is, the raw microprobe data must be multiplied by 1.02 and 1.04, respectively); no correction is required for Na_2O concentrations equal to 2-3 % or less (Laporte et al., 2004). Although the average analytical totals for glasses may be below 98 %, individual analyses not overlapping onto graphite have totals in the range 98 to 99.2 %. The difference to 100 % in the latter analyses is due to the presence of small quantities of additional components not analysed in our standard routine, such as P_2O_5 (up to 2000-3000 ppm), Cl (≈ 1000 ppm at our lowest degrees of melting), CO_2 and water. Glass compositions are given in Table 1; the compositions of all phases and the uncertainties are given in the Supplementary Table S1.

Water in the glassy microdikes of five experiments was measured by secondary ion mass spectrometry (SIMS). The H content was analysed with the CAMECA IMS 4f ion microprobe installed at CNR-IGG, Pavia (Italy), using a -12.5 kV accelerated $^{16}\text{O}^-$ primary beam with a current intensity of 0.5 nA and a beam diameter < 5 μm . The sample mount with that of the standards was left to degas six days in the ion-microprobe sample chamber before analysis. Secondary ion signals of isotopes $^1\text{H}^+$ and $^{30}\text{Si}^+$ (reference isotope for the matrix), in the range of 75–125 eV emission kinetic energies, were monitored at the electron multiplier. Acquisition times were 18 s (H) and 12 s (Si) over three cycles. Secondary ions were detected under steady-state sputtering conditions after 15 min pre-sputtering before true analysis. According to previous SIMS work on hydrogen in silicates, the acquisition of “filtered”

secondary ions is useful in reducing most chemical matrix effects and improving analytical precision (Ottolini et al. 1995 and references therein). Two calibration basaltic glasses, i.e., CY82-29-1V and CLDR (0.09 and 0.16 % H₂O, respectively) were chosen as primary standards to convert H⁺ current intensity into H₂O concentration. In order to correct for the variation of H⁺/Si⁺ signal ratio with varying Fe+Mn+Ti content of each selected area in the sample set, additional standards, such as, schorl no. 16, dravite no. 18, and elbaite no. 19 were used to perform empirical corrections to the relative-to-Si ion yield of hydrogen (for details, see Ottolini and Hawthorne, 2001; Ottolini et al., 2002; Scordari et al., 2010). Overall accuracy is estimated to be of the order of 10 % relative. The water contents (in wt. %) measured in five experiments are as follows: MBK+1, 0.617 ± 0.010 (1- σ); MBK+2, 0.679 ± 0.060 ; MBK3, 1.09 ± 0.06 ; MBK18, 0.528 ± 0.006 ; MBK20, 0.138 ± 0.003 . In addition, a water content equal to 0.621 ± 0.058 wt. % was measured in unpublished experiment MBK8 run at 1 GPa-1200°C ($F = 4.0$ %) with composition MBK using the same technique as Laporte et al. (2004).

2. Melting reactions.

The weight percentages of phases in the run products are given in Table 1. In a plot of the percentage of a solid phase as a function of the percentage of liquid, the slope is equal to the coefficient of that solid phase in the melting reaction (Baker and Stolper, 1994). As the errors on modes are large (Supplementary Table S1), the experimental melting reaction can only be computed with accuracy when melt coexists with the same solid assemblage over a large range of melt fraction. In our study, this is only the case for melt coexisting with ol + opx + cpx + spl in MBK at 1 GPa ($F \approx 5$ to 22 %). In that case, we obtain a melting reaction in which the main reactant is cpx, followed by opx and spl, and ol is on the product side: 0.78

cpx + 0.21 opx + 0.12 spl \rightarrow 1.0 liq + 0.11 ol. This reaction is close to that reported at 1 GPa for fertile peridotites MM3 (Falloon et al., 2008) or FER-E (Pickering-Witter and Johnston, 2000).

3. pMELTS calculations.

3.1 Input parameters. We used the thermodynamic model pMELTS (Ghiorso et al., 2002) and the interface Adibat-1ph (Smith and Asimow, 2005) to compute the equilibrium phase compositions and proportions of partially molten peridotite. The software pMELTS calculates the equilibrium assemblage of phases by minimizing an appropriate potential energy, subject to constraints on bulk composition, temperature, pressure or volume, enthalpy or entropy, and optionally on oxygen fugacity. Ten oxides were taken into account in our calculations: SiO₂, TiO₂, Al₂O₃, Fe₂O₃, Cr₂O₃, FeO, MgO, CaO, Na₂O and K₂O (the latter being treated as a major oxide, not as a trace element). MnO was not included because pMELTS is not calibrated for this element. With Cr₂O₃ set to \approx 0.5 % as in peridotites Bri3, MBK and MBK+ (Table 1), pMELTS strongly overestimated the stability range and the modal proportions of spinel. To solve this problem, Cr₂O₃ was set to 0.1 % in all compositions. The precipitation of leucite, which could occur close to the solidus due to the presence of K₂O, was suppressed in all the calculations because this phase has never been observed in our experiments.

The calculations were made in the isobaric mode with 1°C increments, starting from the superliquidus state. All the calculations were made at FMQ-1 (i.e., the fayalite-magnetite-quartz buffer minus one log unit), close to the oxygen fugacity in our experiments (Laporte et al., 2004). The numerical results are given in the Supplementary Table S2. Three series of calculations were performed to reproduce our experiments with composition MBK at 1 and 1.3 GPa, and composition MBK+ at 1.3 GPa (spreadsheets “MBK 1 GPa”, “MBK 1.3 GPa”,

and “MBK+ 1.3 GPa” in Table S2). A series of calculations was made to study the effect of the bulk K_2O content of peridotite on melt compositions at 1.2 GPa: a series of seven peridotite compositions containing 0, 100, 300, 500, 1000, 1500 and 2000 ppm K_2O was generated starting from a K_2O -free equivalent of our spinel lherzolite Bri3 (see spreadsheet “Effect of K_2O ” for details). Finally, we made two additional sets of calculations dealing with the effect of pressure on the SiO_2 content of low-degree melts and the effect of a non peridotitic source (Supplementary Fig. S2). To address the effect of pressure, we selected the lherzolite composition with 1000 ppm K_2O and we increased P from 1.2 to 2 GPa by steps of 0.1 GPa. The case of a non peridotitic, pyroxene-rich source is discussed below.

3.2 Comparison with MBK series at 1 GPa: evidence for underestimation of plagioclase stability. The experimental series with MBK at 1 GPa is the best suited for a comparison with the pMELTS model as it spans a large range of degrees of melting (from 0.9 to 22.8%). After pl disappearance at $F \approx 5\%$, the model predicts quite accurately the oxide concentrations in liquids (Fig. 2) and the modal proportions of solid phases (Fig. 5a), but the temperatures required to achieve a given melt fraction are 55°C higher than the experimental temperatures. The good agreement on modes and melt compositions for partial melting of peridotite at 1 GPa, and the shift in temperature between pMELTS and experiments have already been reported by Ghiorso et al. (2002) and Smith and Asimow (2005). At low degrees of melting ($F < 5\%$), the theoretical results are not in good agreement with the experimental observations because pl seems to be strongly underestimated by pMELTS: in the model, the pl mode at the solidus is equal to 1.1 %, and pl disappears at $F = 0.7\%$; in the experimental series, the pl mode at the solidus is equal to $\approx 3\%$ (Fig. 1c) and there is still 1.6 % pl at $F = 3.0\%$ (sample MBK16). The discrepancy is important in terms of temperatures and melt

compositions too: according to pMELTS, pl is in equilibrium with liquids strongly enriched in Na₂O (from 7.2 to 8.8 %) at temperatures $\leq 1176^{\circ}\text{C}$, whereas the pl-out temperature in the experiments lies between 1220 and 1240 $^{\circ}\text{C}$, and the experimental plagioclases are in equilibrium with liquids containing 5.6 to 6.1 % Na₂O. Because of the very early disappearance of pl in the model, the proportions of solid phases and the trends of liquid compositions computed at $F < 5\%$ deviate from the observed ones: in particular, the proportions calculated for opx and cpx are overestimated and the proportions of ol and pl are underestimated (Fig. 5a). Finally, as pl in pMELTS is only stable at very low degrees of melting, it is in equilibrium with liquids strongly enriched in Na₂O and K₂O, and depleted in CaO compared to the experimental melts, and thus it has much higher albite and orthoclase contents, and lower anorthite contents than the experimental plagioclases: the theoretical feldspar composition ranges from oligoclase (An₂₅Ab₆₅Or₁₀) at 1176 $^{\circ}\text{C}$ to Ca-K albite (An₁₉Ab₆₀Or₂₁, which is an alkali feldspar as Or > An) at 1156 $^{\circ}\text{C}$ whereas the experimental plagioclases are labradorites ranging from An₅₇Ab₄₁Or₂ at 1220 $^{\circ}\text{C}$ to An₅₄Ab₄₃Or₃ at 1190 $^{\circ}\text{C}$.

3.3 The case of composition MBK+ at 1.3 GPa. The pressure of 1.3 GPa is close to the upper stability limit of plagioclase at the fertile peridotite solidus (Falloon et al., 1999; Till et al., 2012). In the case of MBK+, we expect pl to be stable at the solidus and slightly above because the bulk K₂O content of MBK+ is largely in excess of the amount that could be stored into nominally K₂O-free solid phases such as cpx (which should be less than 100 ppm), and because traces of pl were observed in reversal experiment MBK+13. The program pMELTS finds feldspar in MBK+ at 1.3 GPa, but again we think that it underestimates the stability of this phase. It predicts indeed that feldspar is only stable at very low temperatures and degrees of melting (from the solidus at 1131 $^{\circ}\text{C}$ up to $F \approx 0.6\%$ at 1134 $^{\circ}\text{C}$), and that it is a

K-sanidine ($\text{An}_2\text{Ab}_{20}\text{Or}_{78}$) in equilibrium with liquids with $\text{Na}_2\text{O}+\text{K}_2\text{O} \approx 19.4\%$ and $\text{CaO} = 0.2\%$. We did not find alkali feldspar in our direct partial melting experiments, but we found plagioclase feldspar (K-oligoclase to K-andesine) in the reversal experiments at temperatures up to 1200°C and $\text{Na}_2\text{O}+\text{K}_2\text{O}$ down to 13.7% . The failure of pMELTS to predict feldspar at the right temperature and degree of melting is presumably responsible for the long tail of very low degrees of melting that extends from $\approx 1270^\circ\text{C}$ ($F = 1.63\%$) to 1134°C ($F = 0.63\%$), at which point the crystallization of alkali feldspar leads to complete solidification in less than 3°C . Because pMELTS results at very low degrees of melting are biased by the underestimation of pl stability, we decided to only take into consideration theoretical melts with $\text{Na}_2\text{O}+\text{K}_2\text{O} < 14\%$, assuming that melts with $\text{Na}_2\text{O}+\text{K}_2\text{O} \geq 14\%$ should be saturated with pl as in our reversal experiments (note that the value of $\text{Na}_2\text{O}+\text{K}_2\text{O}$ at which feldspar crystallizes must depend to some extent on pressure and bulk source composition, especially the ratio $\text{K}_2\text{O}/\text{Na}_2\text{O}$). In MBK+ at 1.3 GPa , the criterion $\text{Na}_2\text{O}+\text{K}_2\text{O} < 14\%$ corresponds to $T \geq 1268^\circ\text{C}$ (Supplementary Table S2): this temperature is close to the maximum temperature at which pl is observed in our experiments (1200°C) if we consider a 60°C difference between pMELTS and experimental data (Ghiorso et al., 2002). The theoretical degree of melting at $T = 1268^\circ\text{C}$ ($F = 1.59\%$) is equal to the minimum degree of melting in our experimental series with MBK+ (Table 1).

3.4 Generating phonolite liquids from pyroxene-rich sources. As a starting point, we considered the phase proportions and compositions computed for lherzolite MBK at 1.3 GPa and 1260°C , in which 0.9% of a phonolite liquid (with $\text{SiO}_2 = 54.8\%$ and $\text{Na}_2\text{O} + \text{K}_2\text{O} = 13.9\%$) is in equilibrium with 57.1% ol, 23.1% opx, 16.8% cpx, and 2.3% spl (see spreadsheet “MBK 1.3 GPa” in Table S2). As the same liquid should be in equilibrium with

these four phases whatever their proportions (provided that their compositions remain unchanged), we may anticipate that a phonolite liquid can also be produced from a pyroxene-rich source. To illustrate this point, we computed a bulk composition of pyroxenite, PYROX, by using the same phase compositions as in the above example, but in different proportions: 1 % liquid, 14 % ol, 23 % opx, 60 % cpx, and 2 % spl. The main change is that most ol is replaced by cpx. Composition PYROX is as follows: SiO₂, 50.00 %; TiO₂, 0.32 %; Al₂O₃, 7.48 %; Cr₂O₃, 0.09 %; FeO_{Total}, 5.52 %; MgO, 25.18 %; CaO, 10.42 %; Na₂O, 0.95 %; K₂O, 472 ppm.

The liquid computed for PYROX at 1260°C and 1.3 GPa is almost indistinguishable from the one computed for MBK. With increasing temperature, the oxide concentrations in the liquids from PYROX and MBK become different, but follow the same general trends: for instance, Na₂O decreases with increasing F in both compositions, but it decreases more slowly in composition PYROX because Na₂O is less incompatible due to the abundance of cpx. As expected, liquids strongly enriched in silica and alkalis are produced by partial melting of our pyroxene-rich composition, the most enriched reaching the field of phonolites in the TAS diagram (Supplementary Fig. S2b).

4. Extraction of a phonolite melt from a lherzolite source.

We used a model of melt segregation by compaction (McKenzie, 1989) to estimate how fast a phonolite melt could be extracted from a lherzolite source. In this model, the partially molten source is a uniform layer of thickness h , which rests on an impermeable surface (for instance a subsolidus peridotite). In the initial stage, the melt fraction F_V (equivalent to F , but in vol. %) is assumed to be constant over the whole thickness h . The

driving force of melt extraction is the density contrast between the liquid and its polycrystalline matrix, the liquid being less dense than the matrix. Compaction occurs at the bottom of the partially molten system, and the liquid expelled by compaction at the bottom percolates upwards and forms a layer of extracted liquid at the top of the system. The thickness of the compacting layer at the bottom and that of the liquid layer at the top increase with time.

For given values of h and F_V , the three major parameters controlling the efficiency of melt extraction in this compaction model are the density contrast between melt and matrix, the melt viscosity, and the permeability of the matrix. The time scale of melt extraction, τ , is equal to (McKenzie, 1989):

$$\tau = \frac{h \cdot \mu \cdot F_V}{k \cdot \Delta\rho \cdot g}$$

where μ is the viscosity of the melt, $\Delta\rho$ is the density contrast between matrix and melt, and g is the acceleration due to gravity. The time scale τ is the time taken to separate all but 1/e of the total melt initially present in the partially molten layer: at time τ , the thickness of the melt layer at the top is equal to $0.632 \cdot h \cdot F_V$.

At $T \approx 1200-1250^\circ\text{C}$, our phonolite liquids have viscosities of the order of 10^3 Pa·s in the absence of water, and 10^2 Pa·s with 1 % dissolved water (Giordano et al., 2008). Low-degree melts of a fertile mantle are expected to contain some water, so we use viscosities of the order of 10^2 Pa·s in the calculations. Pressure is not taken into account in Giordano's et al. model, but the variation of viscosity with pressure is expected to be small (Del Gaudio and Behrens, 2009). At 1-1.5 GPa and 1200-1250°C, the density of phonolite liquids is 2550 kg/m³ in the absence of water, and 2450 kg/m³ with 3 % dissolved H₂O (Seifert et al., 2013). In the calculations, we use 2500 kg/m³ and 3200 kg/m³ for melt and matrix density,

respectively. Permeability (k , m^2) was computed as a function of melt fraction per unit volume, F_V , and grain diameter a ($a \approx 10^{-3}$ m) using the relationship (McKenzie, 1989):

$$k = \frac{a^2 \cdot F_V^2}{3000}$$

Compaction calculations were performed for four lherzolite sources with different bulk K_2O contents: 100, 300, 1000, and 2000 ppm K_2O . For each source, we computed melt compositions as a function of decreasing melt fraction with the software pMELTS (see the spreadsheet “Effect of K_2O ” in Supplementary Table 2), and we selected the phonolite composition with $\text{Na}_2\text{O}+\text{K}_2\text{O} = 14$ %. The calculations were made for a partially molten layer of thickness $h = 1000$ m. The variables and the results are summarized in the two tables below.

Bulk K_2O	T ($^\circ\text{C}$)	wt. % liq	SiO_2	TiO_2	Al_2O_3	Cr_2O_3	FeO	MgO	CaO	Na_2O	K_2O
100 ppm	1227	0.27	55.05	0.55	20.97	0.01	2.24	4.75	2.37	10.38	3.69
300 ppm	1235	0.66	55.63	0.56	20.91	0.01	2.08	4.46	2.35	9.43	4.57
1000 ppm	1250	1.57	56.83	0.59	20.81	0.00	1.72	3.80	2.22	7.64	6.39
2000 ppm	1264	2.58	57.70	0.61	20.72	0.00	1.48	3.35	2.13	6.27	7.74

Fractions and compositions of phonolite melts used in the compaction model. Temperature, melt fractions and melt compositions are the results of pMELTS calculations for four different lherzolite sources (with 100, 300, 1000, and 2000 ppm K_2O). For each source, the selected melt composition is the one with $\text{Na}_2\text{O}+\text{K}_2\text{O} = 14$ %.

Bulk K_2O	F	F_V	Viscosity	Permeability	Time τ	Thickness h
	wt. %	vol. %	Pa·s	m^2	year	m
100 ppm	0.27	0.35	81	4.0×10^{-15}	3.2×10^5	2.2
300 ppm	0.66	0.84	97	2.3×10^{-14}	1.6×10^5	5.3
1000 ppm	1.57	2.00	146	1.3×10^{-13}	1.0×10^5	12.6
2000 ppm	2.58	3.28	192	3.6×10^{-13}	8.1×10^4	20.7

Time scales of melt extraction, τ , and thickness, h , of the layer of segregated melt; the thickness of the partially molten source is equal to 1000 m. Parameters F and F_V are the melt fractions in wt. % and vol. %, respectively. The viscosity was computed using the model of Giordano et al. (2008), assuming 1 wt. % dissolved H_2O in the phonolite melts. Permeabilities are computed for a grain size of 1 mm.

References

- Baker M. B. and Stolper E. M., 1994. Determining the composition of high-pressure mantle melts using diamond aggregates. *Geochim. Cosmochim. Acta*, 58: 2811-2827.
- Del Gaudio P. and Behrens H., 2009. An experimental study on the pressure dependence of viscosity in silicate melts. *J. Chem. Phys.*, 131: 044504; doi: 10.1063/1.3169455
- Falloon T. J., Green D. H., Danyushevsky L. V. and Faul U. H., 1999. Peridotite melting at 1.0 and 1.5 GPa: an experimental evaluation of techniques using diamond aggregates and mineral mixes for determination of near-solidus melts. *J. Petrol.*, 40: 1343-1375.
- Falloon T. J., Green D. H., Danyushevsky L. V. and McNeill A. W., 2008. The composition of near-solidus partial melts of fertile peridotite at 1 and 1.5 GPa: Implications for the petrogenesis of MORB. *J. Petrol.*, 49: 591-613.
- Ghiorso M. S., Hirschmann M. M., Reiners P. W. and Kress V. C. III, 2002. The pMELTS: A revision of MELTS for improved calculation of phase relations and major element partitioning related to partial melting of the mantle to 3 GPa. *Geochem. Geophys. Geosyst.*, 3: art. no. 1030, doi:10.1029/2001GC000217.
- Giordano D., Russell J. K. and Dingwell D. B., 2008. Viscosity of magmatic liquids: A model. *Earth Planet. Sci. Lett.*, 271: 123-134. McKenzie, 1989.
- Lambart S., Laporte D. and Schiano P., 2009. An experimental study of focused magma transport and basalt-peridotite interactions beneath mid-ocean ridges: Implications for the generation of primitive MORB compositions. *Contrib. Mineral. Petrol.*, 157: 429-451.
- Laporte D., Toplis M., Seyler M. and Devidal J-L., 2004. A new experimental technique for extracting liquids from peridotite at very low degrees of melting: Application to partial melting of depleted peridotite. *Contrib. Mineral. Petrol.*, 146 : 463-484.
- Luth W. C. and Ingamells C. O., 1965. Gel preparation of starting materials for hydrothermal experimentation. *Amer. Mineral.*, 50: 255-258.

- McKenzie D., 1989. Some remarks on the movement of small melt fractions in the mantle. *Earth Planet. Sci. Lett.*, 95: 53-72.
- Ottolini L., Bottazzi P., Zanetti A. and Vannucci R., 1995. Determination of hydrogen in silicates by secondary ion mass spectrometry. *Analyst*, 120: 1309-1313.
- Ottolini L. and Hawthorne F. C., 2001. SIMS ionization of hydrogen in silicates: A case study of kornerupine. *J. Anal. At. Spectrom.*, 6: 1266-1270.
- Ottolini L., Cámara F., Hawthorne F. C. and Stirling J., 2002. SIMS matrix effects in the analysis of light elements in silicate minerals: Comparison with SREF and EMPA data. *Amer. Mineral.*, 87: 1477-1485.
- Pickering-Witter J. and Johnston A. D., 2000. The effects of variable bulk composition on the melting systematics of fertile peridotitic assemblages. *Contrib. Mineral. Petrol.*, 140: 190-211.
- Scordari F., Dyar M. D., Schingaro E., Lacalamita M. and Ottolini L., 2010. XRD, micro-XANES, EMPA, and SIMS investigation on phlogopite single crystals from Mt. Vulture (Italy). *Amer. Mineral.*, 95: 1657-1670.
- Seifert R., Malfait W. J., Petitgirard S. and Sanchez-Valle C., 2013. Density of phonolitic magmas and time scales of crystal fractionation in magma chambers. *Earth Planet. Sci. Lett.*, 381: 12-20.
- Smith P. M. and Asimow P. D., 2005. Adibat_1ph: A new public front-end to the MELTS, pMELTS, and pHMELTS models. *Geochem. Geophys. Geosyst.*, 6: art. no. Q02004, doi:10.1029/2004GC000816.
- Till C. B., Grove T. L. and Krawczynski M. J., 2012. A melting model for variably depleted and enriched lherzolite in the plagioclase and spinel stability fields. *J. Geophys. Res.*, 117: B06206. Amer. Geophys. Union.

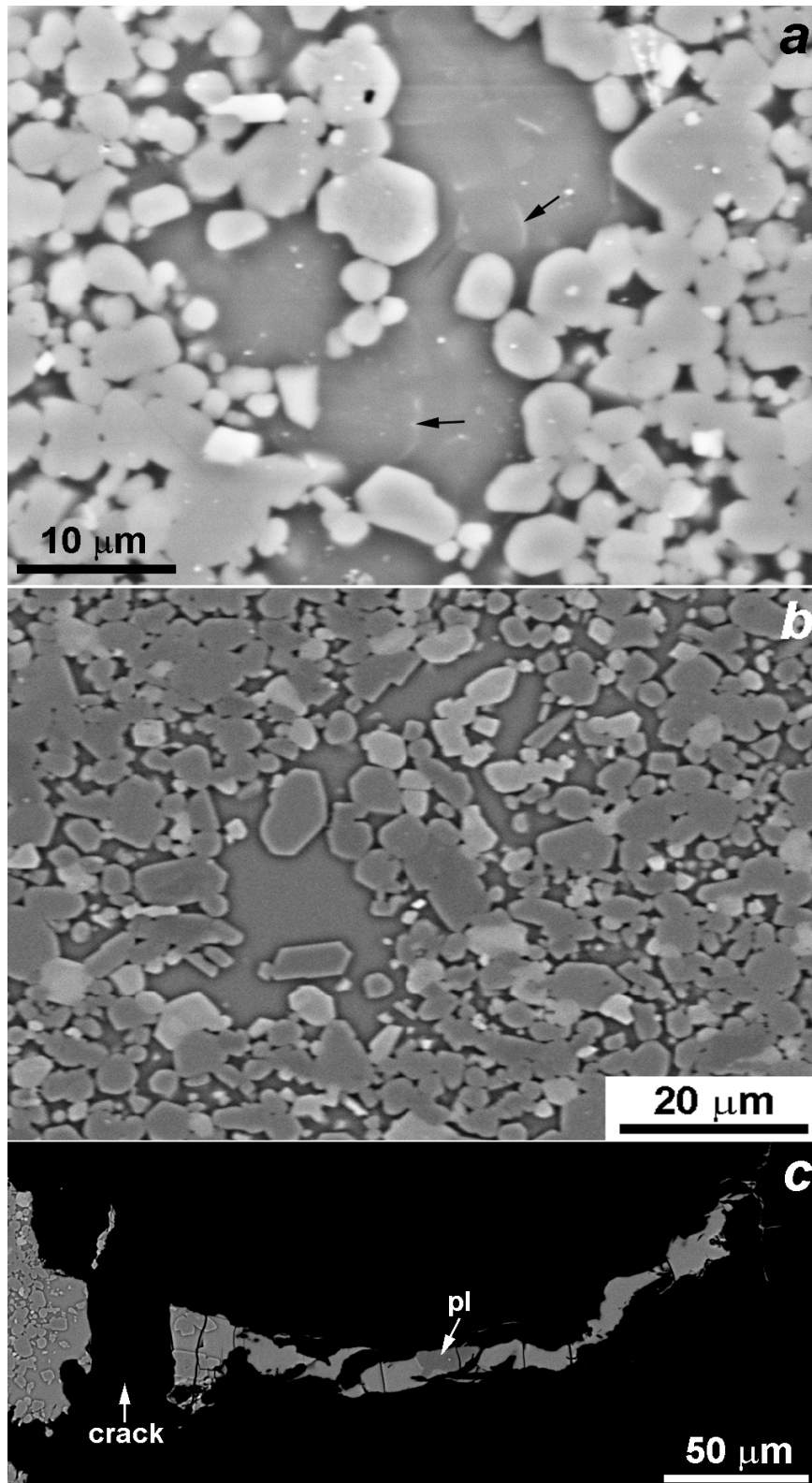


Figure S1. SEM-Backscattered electron microphotographs of reversal experiments MBK+13 and MBK+14. (a) Sample MBK+14 (1.3 GPa-1180°C) is a partially molten spl + pl lherzolite showing melt pockets crowded with small plates of pl (K-oligoclase; arrows). (b) The overall texture of sample MBK+13 (1.3 GPa-1200°C) is similar to MBK+14 except that the melt pockets are devoid of plagioclase. (c) The only trace of pl in MBK+13 is an aggregate of a few crystals in a microdike.

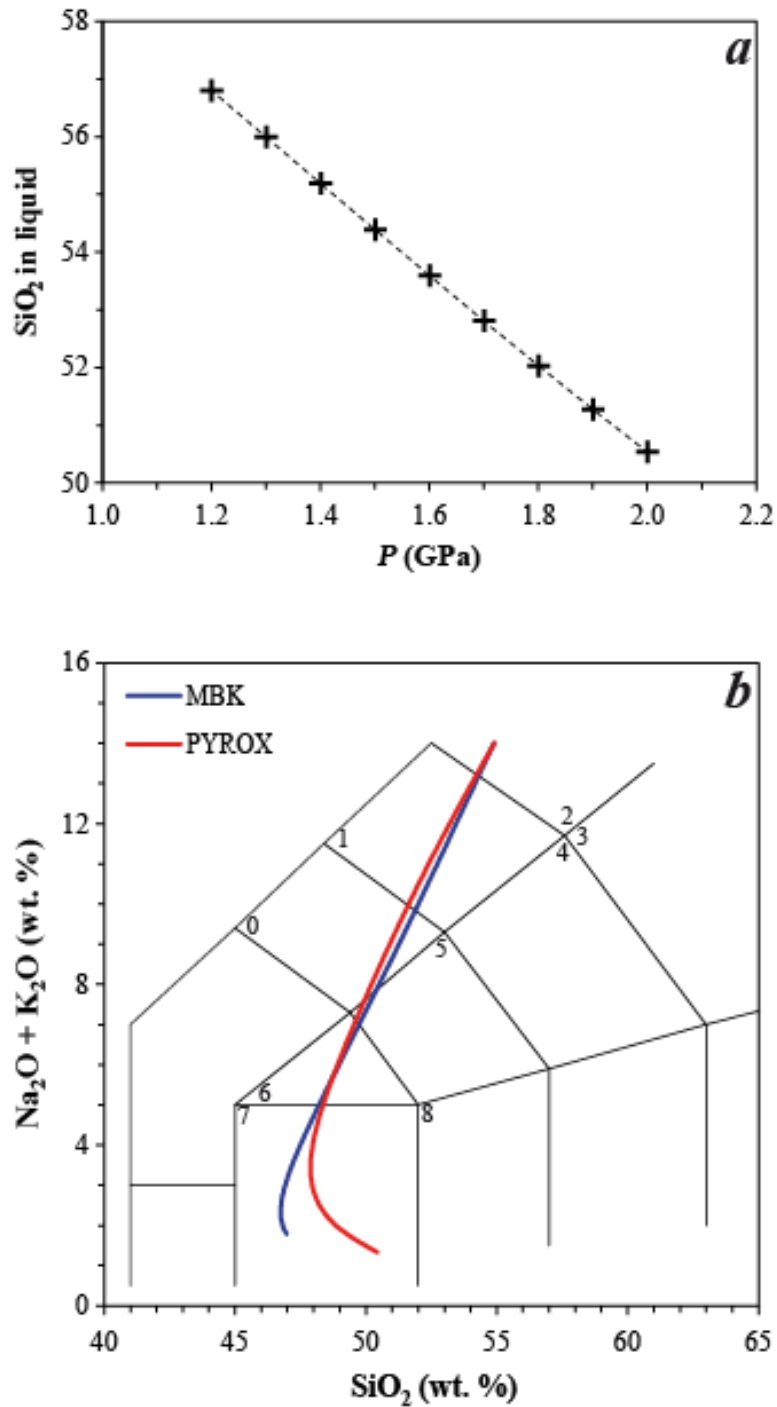


Figure S2. (a) Evolution of SiO₂ in low-degree melts as a function of pressure (at each pressure, we selected the melt composition with Na₂O+K₂O = 14 %; the selected compositions correspond to a nearly constant melt fraction: $F = 1.6\%$). (b) TAS diagram showing the melts produced by partial melting of lherzolite MBK and pyroxenite PYROX at 1.3 GPa; the trends extend from 1260°C ($F \approx 1\%$) to the cpx-out temperature ($F = 21.6\%$ in MBK; $F = 75.0\%$ in PYROX). Labels are as follows: (0) Phonotephrite; (1) Tephriphonolite; (2) Phonolite; (3) Trachyte; (4) Trachyandesite; (5) Basaltic trachyandesite; (6) Trachybasalt; (7) Basalt; (8) Basaltic andesite.

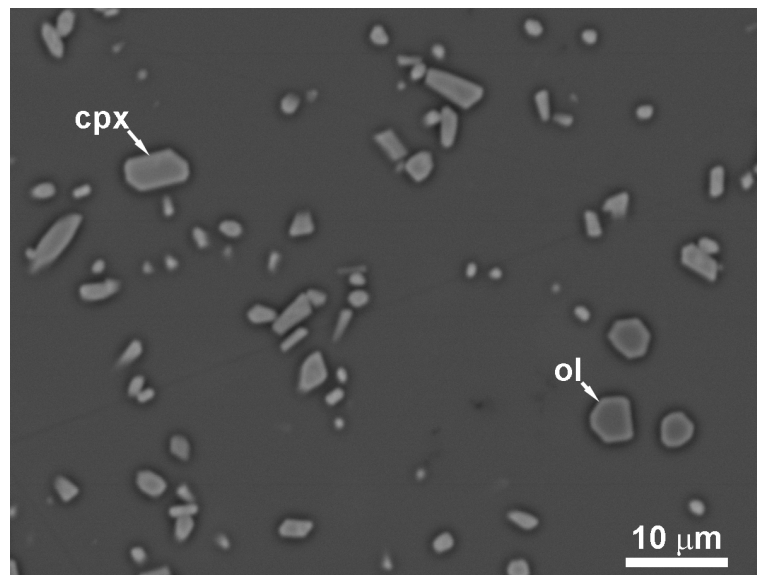


Figure S3. SEM-Backscattered electron microphotograph showing the texture and paragenesis of phonolite gel +6 equilibrated at 1 GPa-1150°C (crystallization experiment CrysPho2): equant grains of olivine and more elongated grains of clinopyroxene (slightly brighter) are dispersed into a darker glassy matrix.